Geosci. Model Dev. Discuss., 8, 3079–3115, 2015
www.geosci-model-dev-discuss.net/8/3079/2015/
doi:10.5194/gmdd-8-3079-2015

Geoscientific Model Development Discussions
Open Access

OESbathy version 1.0: a method for reconstructing ocean bathymetry with realistic continental shelf-slope-rise structures

A. Goswami[1], P. L. Olson[1], L. A. Hinnov[1,*], and A. Gnanadesikan[1]

[1]Department of Earth and Planetary Sciences, Johns Hopkins University, Baltimore, Maryland, USA
[*]now at: Department of Atmospheric, Oceanic, and Earth Sciences, George Mason University, Fairfax, Virginia, USA

Received: 12 February 2015 – Accepted: 14 March 2015 – Published: 2 April 2015

Correspondence to: A. Goswami (arghya.goswami@jhu.edu)

Published by Copernicus Publications on behalf of the European Geosciences Union.

Abstract

We present a method for reconstructing global ocean bathymetry that uses a plate cooling model for the oceanic lithosphere, the age distribution of the oceanic crust, global oceanic sediment thicknesses, plus shelf-slope-rise structures calibrated at modern active and passive continental margins. Our motivation is to reconstruct realistic ocean bathymetry based on parameterized relationships of present-day variables that can be applied to global oceans in the geologic past, and to isolate locations where anomalous processes such as mantle convection may affect bathymetry. Parameters of the plate cooling model are combined with ocean crustal age to calculate depth-to-basement. To the depth-to-basement we add an isostatically adjusted, multicomponent sediment layer, constrained by sediment thickness in the modern oceans and marginal seas. A continental shelf-slope-rise structure completes the bathymetry reconstruction, extending from the ocean crust to the coastlines. Shelf-slope-rise structures at active and passive margins are parameterized using modern ocean bathymetry at locations where a complete history of seafloor spreading is preserved. This includes the coastal regions of the North, South, and Central Atlantic Ocean, the Southern Ocean between Australia and Antarctica, and the Pacific Ocean off the west coast of South America. The final products are global maps at $0.1^{\circ} \times 0.1^{\circ}$ resolution of depth-to-basement, ocean bathymetry with an isostatically adjusted, multicomponent sediment layer, and ocean bathymetry with reconstructed continental shelf-slope-rise structures. Our reconstructed bathymetry agrees with the measured ETOPO1 bathymetry at most passive margins, including the east coast of North America, north coast of the Arabian Sea, and northeast and southeast coasts of South America. There is disagreement at margins with anomalous continental shelf-slope-rise structures, such as around the Arctic Ocean, the Falkland Islands, and Indonesia.

GMDD

8, 3079–3115, 2015

1 Introduction

Reconstructing paleobathymetry represents a challenge in modelling past climates. Under modern continental distributions, high-latitude bathymetry modulates global climate by blocking flow through Drake Passage, which may have impacts on the magnitude of the circumpolar current (Krupitsky et al., 1995), or in changing the stability of the thermohaline circulation (Sijp and England, 2005). Similarly, in the Northern Hemisphere changes in the depth of the Greenland–Iceland–Scotland Ridge have been proposed to play a role in modulating North Atlantic Deep Water formation (Wright and Miller, 1996). Generation of tides over rough ocean bottoms is thought to play a major role in driving deep ocean mixing (Simmons et al., 2004).

Examining such processes under past climate, however, is difficult. Analysis of the distribution of ages for the modern oceanic crust reveals that 46 % of the crust is younger than 50 Ma, 31 % is 51 to 100 Ma old, and the remaining 23 % is older than 100 Ma (Müller et al., 2008). Because older ocean crust is recycled through subduction processes, direct reconstruction of bathymetry for the paleo-ocean is problematic. Apart from benthic fossil and sediment paleo-depth interpretations (Holbourn et al., 2001), there is little by way of a geologic record to quantify paleobathymetry where ocean crust has been subducted.

The past decade has witnessed vast improvement in the quality of high-resolution global ocean bathymetry, ocean sediment thickness, and ocean crustal age data, important refinements to models of the lithosphere. These advancements provide an opportunity to revisit the question of what the ocean bottom looked like in the past. In this work we apply these new data and modeling tools to develop a method that can be used to extend ocean bathymetry back through geologic time. Modern ocean bathymetry, sediment thickness, and continental shelf-slope-rise structure are parameterized to reconstruct a realistic ocean bathymetry, tied to age of the oceanic crust and idealized representations of marginal marine sediment structures. We name this

GMDD
8, 3079–3115, 2015

reconstructed bathymetry "OESbathy", abbreviated to OES for this paper (OES = Open Earth Systems; www.openearthsystems.org).

Modern ocean bathymetry reconstructed through this methodology is used as a test case, as it offers the following advantages: (1) differences can be assessed between actual ocean bathymetry and the reconstruction, (2) when applied to coupled climate models, it can be used to assess the influence of the reconstruction with respect to actual ocean bathymetry, and (3) quantitative confidence levels can be developed for the reconstruction. Additionally, the differences between the actual and reconstructed bathymetry can be used to examine the impact of processes such as sedimentation and dynamic topography on climate.

2 Data

For the age distribution of the oceanic crust (hereafter ocean crust age is represented by τ) we use the data from Müller et al. (2008; earthbyte.org). Here we use the term "age" with two different meanings. Crustal age refers to the age of the oceanic crust relative to its time of formation, whereas reconstruction age refers to the geologic time for which the reconstruction is made. Müller et al. (2008) presented global reconstructions of oceanic crustal age in one million year intervals for the past 140 million years. For each reconstructed age in Müller et al. (2008), age of the oceanic crust, depth-to-basement, and bathymetry are given. The age of the oceanic crust is given in million years before present (Ma). The depth-to-basement (ω_τ), defined as the distance between mean sea level and the top of the basaltic layer of the oceanic crust, and bathymetry, defined as the distance between mean sea level and sea floor, are expressed in meters. The reconstructed bathymetry from Müller et al. (2008) is referred to hereafter as EB08 (EB = EarthByte). The geographic coordinates are in decimal degrees, and the data are in $0.1^\circ \times 0.1^\circ$ resolution (3601 longitude × 1801 latitude points). For this project, 000 Ma (modern) crustal age reconstruction data are used (Fig. S1).

GMDD
8, 3079–3115, 2015

We use modern ocean sediment thickness data from Divins (2003). These data are derived from seismic profiling of the world's ocean basins and other sources. The reported thicknesses are calculated using seismic velocity profiles that yield minimum thicknesses. Data values are in meters and represent the distance between sea floor and "acoustic basement". These data are given in $5' \times 5'$ resolution and have been re-gridded to $0.1^\circ \times 0.1^\circ$ resolution values (Fig. S2), to match the EB08 crustal age grid.

To construct the marginal marine shelf-slope-rise structures, ETOPO1 modern bathymetry (Amante and Eakins, 2009) is used. These data give the distance between the Earth's solid surface and mean sea level in meters, including land topography and ocean bathymetry, from numerous global and regional sources. We use the "Bedrock" version of ETOPO1, which is available in a $1' \times 1'$ resolution (earthmodels.org) and has been re-gridded to $0.1^\circ \times 0.1^\circ$ resolution (Fig. S2) in order to match the EB08 crustal age grid (Fig. S3). This version of ETOPO1 provides relief of earth's surface depicting the bedrock underneath the ice sheets. However, we use only the oceanic points in this dataset, so that this has no impact on the reconstructed bathymetry.

3 Methods

Modern ocean basins have different types of crust, including oceanic crust, submerged continental crust, and transitions between these two types. In our reconstruction, the regions underlain by oceanic crust to which a crustal age has been assigned are termed "open ocean" regions. The parts of the ocean basins that occupy the transitional zone between oceanic crust and the emerged continental crust are termed "shelf-slope-rise" regions. These regions typically extend from the boundary of open ocean regions to the coastline. Accordingly, the OES ocean bathymetry model involves the merging of open ocean regions and shelf-slope-rise regions (Fig. 1). To accomplish the merging, map-based operations such as computing distances between locations were carried out in ArcGIS 10.1, whereas local calculations such as interpolation and statistics were carried out in Matlab R2014a.

GMDD
8, 3079–3115, 2015

3.1 Reconstruction of open ocean regions

Reconstruction of open ocean bathymetry starts with age of the oceanic crust. This information is available only at locations where oceanic crust is preserved or has been reconstructed. Calculation of ocean depth-to-basement is based on a cooling plate model in which the vertical distance between mean sea level and basement ω_τ is expressed as:

$$\omega_\tau = \omega_0 + \omega_d \tag{1}$$

where the $\omega_0 = -2639.8$ m is the area-weighted average of mid-oceanic ridge depths from the North Pacific, Eastern Atlantic and Southeast Atlantic reported in Crosby et al. (2006), and ω_d is the change in depth due to plate cooling. Here we adopt a negative sign to denote depths below mean sea level. The change in depth due to cooling of the oceanic plate ω_d is given by (adopted from Eq. 4.213 in Turcotte and Schubert, 2002):

$$\omega_d = \frac{-\alpha\rho_m(T_m - T_w)y_L}{(\rho_m - \rho_w)}\left[\frac{1}{2} - \frac{4}{\pi^2}\sum_{m=0}^{\infty}\frac{1}{(1+2m)^2}\exp\left(\frac{-\kappa}{y_L^2}(1+2m)^2\pi^2\tau\right)\right] \tag{2}$$

where α is the volumetric coefficient of thermal expansion of the mantle, ρ_m is density of the upper mantle, ρ_w is density of sea water, $T_m - T_w$ is difference between upper mantle and ocean temperature, κ is thermal diffusivity, y_L is equilibrium plate thickness, all assumed to have constant values.

The equilibrium depth-to-basement ω_e corresponds to the limit of $\tau \to \infty$ in Eq. (2), appropriate for the oldest crust:

$$\omega_e = \frac{-\alpha\rho_m(T_m - T_w)y_L}{2(\rho_m - \rho_w)}. \tag{3}$$

In our reconstruction we use $\omega_e = -5875$ m, the mid-point of the range -5750 to -6000 m in the oldest part of the North Pacific (Crosby et al., 2006). Similarly we assign

GMDD
8, 3079–3115, 2015

an area-weighted average value to the parameter β:

$$\beta = \frac{2\alpha\rho_m(T_m - T_w)}{(\rho_m - \rho_w)}\sqrt{\frac{\kappa}{\pi}} = 329.5\,\mathrm{m\,s^{-\frac{1}{2}}} \quad (4)$$

so that

$$\frac{\kappa}{y_L^2} = \left(\frac{\beta\sqrt{\pi}}{2\omega_e}\right)^2 = 4.97\times10^{-2}\,\mathrm{s^{-1}}. \quad (5)$$

In terms of ω_e and β, Eq. (2) becomes

$$\omega_d = \omega_e\left[\frac{1}{2} - \frac{4}{\pi^2}\sum_{m=0}^{\infty}\frac{1}{(1+2m)^2}\exp\left(\frac{-\beta\sqrt{\pi}}{2\omega_e^2}(1+2m)^2\pi^2\tau\right)\right]. \quad (6)$$

We include the first 25 terms in the sum of Eq. (6) to ensure convergence. Lastly, the depth-to-basement is calculated with Eq. (1).

3.2 Modeled sediment layer and isostatic correction

A parameterized multicomponent sediment layer, called "OES sediment thickness" (Figs. 2 and 3), was isostatically added on top of the depth-to-basement ω_τ; (Fig. 4) to complete the open ocean bathymetry (Fig. 5). OES sediment thickness was parameterized based on a third degree polynomial fit between area corrected global sediment thickness data (Whittaker, 2013) and age of the underlying oceanic crust τ (Fig. 3). Sediment loading was calculated using a multicomponent sediment layer with varying sediment densities given in Table 2 in 100 m increments of the sediment. The variable sediment densities were calculated from a linear extrapolation of sediment densities in Crosby et al. (2006) (Table S1). For the isostatic correction, in each 100 m sediment layer we calculate an adjusted thickness given by

$$D_z = \frac{100(\rho_m - \rho_z)}{(\rho_m - \rho_w)} \quad (7)$$

GMDD
8, 3079–3115, 2015

where ρ_z is the density of the zth layer, $\rho_m = 3300\,kg\,m^{-3}$ and $\rho_w = 1000\,kg\,m^{-3}$. The sediment model has a total of 16 layers in which the basal layer includes all sediment deeper than 1500 m. For a given location we sum D_z to obtain the isostatically adjusted total sediment thickness, which is then added to the depth-to-basement to obtain the open ocean bathymetry. This unloading correction is similar to unloading procedures used by Crough (1983) and Sykes (1996).

3.3 Reconstruction of shelf-slope-rise structures

To model the shelf-slope-rise structure, profiles from various modern shelf-slope-rises at active and passive margin regions from ETOPO1 were examined, along with their corresponding sediment thicknesses taken from Divins (2003). As a representative active margin, the west coast of South America was chosen (Fig. 6). For passive margins, the Atlantic Ocean (north, south and central) and part of the Southern Ocean were chosen as representatives, because their complete rifting history is preserved (Figs. 7 and S4).

Profiles from these representative regions were used to parameterize the widths of the continental shelf, slope and rise as follows. The basic parameters of the shelf-slope-rise structure (Fig. 8a) include continental shelf width l_{sh}, continental slope width l_{sl}, and continental rise width l_r. The location of the maximum extent of oceanic crust according to EB08 is labeled as M, and another anchor point labeled as P marks the boundary between the shelf-slope-rise structure and the open ocean. These are related by:

$$l_{sh} + l_{sl} = M \tag{8a}$$

$$l_{sh} + l_{sl} + l_r = P \tag{8b}$$

$$l_r = -0.290 l_{sl} + 437.2 \tag{8c}$$

$$l_{sl} + l_r = -8.28 \times 10^{-3} l_{sh}^2 + 5.486 l_{sh}, \tag{8d}$$

where M and P are the distances of coastline from points M and P, respectively.

GMDD
8, 3079–3115, 2015

The numerical coefficients in Eqs. (8a)–(8d) were obtained from fits to ETOPO1 profiles (Fig. 8b and c). To determine the corresponding depths, we work outward from the coast. First we apply a uniform gradient of 3.2° in depth over the width of the shelf. This value of the shelf gradient was obtained from analysis of 17 ETOPO1 transects (Figs. S4 and S5). For the depth distribution along the slope and rise, we assume another uniform gradient as illustrated in Fig. 8a, joining the depth at the shelf break with the depth calculated for the open ocean at point P.

This methodology works for all shelf-slope-rise regions except where the shelf is anomalously extended, for example, north of Siberia, the Falkland Islands region, and the complex regions in Southeast Asia. If the M point is too far from the coastline, so that $l_{sh} + l_{sl} > 800$ km, or too close to the coastline, so that $l_{sh} + l_{sl} < 100$ km, then the relationship among the three widths no longer holds. For these regions we assume that $P = M$ (Fig. 1c). To complete the reconstruction, these regions were filled by interpolation from neighboring regions.

4 Results

4.1 Reconstructed shelf-slope-rise structures

ETOPO1 bathymetry reveals that active margins lack extensive shelves (Fig. 4), and their slope gradient is anomalously large. Likewise, sediment thickness profiles show that active margins have little sediment cover, either near or far from the coast. In particular, sediment thickness on the shelves of active margins rarely exceeds 250 m and gradually thins out beyond the subduction zone towards the open ocean.

In contrast to active margins, passive margins are characterized by the presence of significant shelf regions. Three out of the sixteen passive margin cross sections studied are shown in Fig. 7. The extent of the shelf region varies substantially along passive margin coastlines, which accounts for the scatter between the profiles in Fig. 7. For example, in the profile between the southern tip of Africa and South America, the

GMDD
8, 3079–3115, 2015

South American side has a very wide, platform-like shelf region that extends for more than 500 km, whereas on the African side the shelf is at most 100 km wide.

The bathymetric gradients at passive continental margin slopes in Fig. S5 vary significantly, from −0.003 to −0.018. Compared to active margins, passive margins are characterized by greater thickness of sediments and more lateral variability. The greater sediment thickness on passive margins and its greater lateral variability are evident in the thirteen passive margin transects shown in Fig. S4.

Figure 8 shows the relationship between the widths of the shelves and the corresponding slope-plus-rise structure. A transect east/northeast of Newfoundland in the northern part of the Atlantic Ocean (Fig. S4c, top center panel) includes a 300 km of continental shelf and nearly 900 km of continental slope-plus-rise. The presence of the widely extended Gulf of St. Lawrence may contribute to this anomaly.

4.2 Reconstructed open ocean regions

Our depth-to-basement reconstruction is shown in Fig. 4. The isostatically adjusted, sediment-loaded model bathymetry of the open ocean is shown in Fig. 5, for which only ocean basin areas with ocean crust ages have an assigned bathymetry. The gap between the coastline and open ocean bathymetry is reconstructed with the shelf-slope-rise model described in Sect. 3.3.

The mid-oceanic ridge systems in our open ocean bathymetry in Fig. 4 have an average depth of approximately −2675 m. Away from the mid-ocean ridges, ocean depth increases systematically, and reaches a maximum depth of approximately −5575 m at old crustal ages. In Fig. 5, the open ocean bathymetry is shown with the modeled sediment cover from Fig. 3 isostatically loaded on to it. With this sediment cover added, the bathymetry ranges between −2675 to −4900 m in the open ocean regions and the maximum depth of the reconstructed bathymetry is approximately −6500 m. The depth range between −4900 and −6500 m is associated with old ocean crust (crustal age in the range of τ = 100–120 Ma) along the flanks of the Atlantic, Pacific, Southern and Indian Oceans, and the Bay of Bengal.

GMDD
8, 3079–3115, 2015

4.3 Model evaluation

The addition of the shelf-slope-rise model completes the OES bathymetry (Fig. 9), except for ocean islands, seamounts, trenches, plateaus and other localized anomalies plus the underlying dynamical topography. Below we evaluate the modeled OES bathymetry with respect to the ETOPO1 and EB08.

4.3.1 Statistics

Basic statistics of the OES, ETOPO1 and EB08 bathymetries are summarized in Table 3. Compared to the −10 714 m maximum depth of ETOPO1, OES maximum depth is −6522 m, while the deepest point of EB08 is only −5267 m. These differences from ETOPO1 are due to the absence of trenches in the reconstructions. The average ocean depths for the ETOPO1, OES and EB08 bathymetries are −3346, −3592 and −4474 m, respectively, signifying that EB08 in particular is very deep compared to ETOPO1. The SD of the ETOPO1, OES and EB08 bathymetries are 1772.25, 1668.52 and 785.08 m, respectively. These values suggest that compared to ETOPO1, the EB08 is overall very smooth, whereas OES bathymetry has a variability that is comparable to ETOPO1.

We also assessed the skewness and kurtosis of the three bathymetries. Skewness is a measure of the asymmetry of data around their mean, and is zero for a symmetric distribution. The skewness of OES bathymetry (1.34) lies between ETOPO1 (0.67) and EB08 (1.81), indicating a closer fit of OES to ETOPO1 than EB08 to ETOPO1. Kurtosis is a measure of how outlier-prone a distribution is. Kurtosis equals to 3 for a Normal distribution, whereas outlier-prone distributions have a kurtosis greater than 3, and less outlier-prone distributions have kurtosis less than 3. For the three bathymetries the kurtosis values are 2.30 (OES), 3.26 (ETOPO1) and 7.69 (EB08), respectively. It should be noted that the OES bathymetry does not take into account large igneous provinces (LIPs), seamounts, or plateaus, whereas EB08 has incorporated some of the major LIPs.

GMDD
8, 3079–3115, 2015

4.3.2 Difference maps

To assess the quality of our results, we difference OES from ETOPO1 bathymetry in Fig. 10, with positive values corresponding to regions where OES is deeper than ETOPO1 and negative values corresponding to regions where OES is shallower than ETOPO1. As described in Sect. 3, interpolations were used in certain regions to complete the reconstruction, for examples, the Falkland Island regions, north of Siberia, and the complex regions around SE Asia. These regions show significant deviations from ETOPO1; in general, OES is much deeper. Some shelf-slope-rise structures are shallower in OES than ETOPO1, such as around the margins of the central Atlantic, whereas in other areas OES is deeper, such as along the east coast of Africa, the Bay of Bengal and the Arctic Ocean margin. Owing to the absence of seamounts and plateaus in OES bathymetry, those areas display large positive anomalies.

A difference map between the OES sediment thickness (Fig. 3) and the Divins (2003) global ocean sediment (Fig. S2) has been calculated for the open ocean regions. Figure S6 shows that the most noticeable differences occur close to the continent margins (edge of the ocean crust), where large negative values indicate that the modeled sediment thicknesses are much less than actual sediment thicknesses. Otherwise, over a substantial part the open ocean, especially on ridge flanks, the differences in Fig. S6 are close to zero, indicating a good fit between the OES parameterized and Divins (2003) sediment thickness. In the Atlantic abyssal plains, however, OES sediment thickness generally exceeds the Divins (2003) sediment thickness. Likewise, OES sediment thickness exceeds measured sediment thickness (up to 0.5 km) in the eastern Indian Ocean (offshore Australia) and significantly exceeds (by more than 1 km) measured sediment thickness throughout the western Pacific Ocean.

4.3.3 Shelf-slope-rise profiles

Shelf-slope-rise cross sections from all continents, here referred to as “lines” are compared using OES, EB08 and ETOPO1 bathymetries (Figs. 11 and S7). The lines shown

GMDD
8, 3079–3115, 2015

in Fig. 11b, c, g, and j agree well with ETOPO1, while those in Fig. 11d and e are partial fit, and the lines in Fig. 11f, h, and i are poor fits. In all lines, EB08 bathymetry is shown only for the deep oceans with no continental shelf or slope, and as a result none of the EB08 lines reach the coast. Of the 64 lines depicted, nearly 50 % fit well with ETOPO1.

Along Line 1 from the North Pacific (Fig. 11b), the OES bathymetry is in good agreement with the ETOPO1 bathymetry, especially for the shelf and slope. Beyond 550 km, OES bathymetry is deeper and lacks the local variations of ETOPO1, such as from the seamounts. EB08 bathymetry is even deeper than OES along this line with a similar lack of local variation. Along the northeast coast of South America and Australia (Fig. 11c and g), Lines 12 and 39, OES bathymetry agrees with ETOPO1, whereas the EB08 bathymetry is deeper than both OES and ETOPO1. Figure 11j shows Line 61 off the coast of Delaware, USA. Here, there is good agreement between ETOPO1 and OES from the shelf-slope-rise to the open ocean region out to ~ 600 km distance from the coast.

Lines 20 and 22 (Fig. 11d and e) are taken from coastal Nigeria and the southern tip of Africa. Here, OES bathymetry has a partial fit with ETOPO1. The OES shelf in both lines is wider than ETOPO1, and as a result, the OES slope + rise is too steep. However, the fit improves in the open ocean along both lines.

Lines 58 and 60 (Fig. 11h and i) are from the northern part of Eurasia. This region was filled in by interpolation from nearby regions, because it has a hyper-extended shelf that our parameterization fails to model. Hence, along these two lines there is poor agreement between ETOPO1 and OES. The ETOPO1 shelf is very shallow (< 1000 m below sea level), whereas the OES shelf is deeper with a steeper gradient on the slope-rise. Similar deviations occur in Line 33 (Fig. 11f) from the Bay of Bengal, where an enormous pile of sediment from the Ganges system has accumulated, resulting in a much shallower ETOPO1 compared to OES.

GMDD
8, 3079–3115, 2015

5 Discussion

5.1 Shelf-slope-rise internal architecture

Examples of the global ocean sediment thickness data of Divins (2003) are displayed as cross-sectional profiles from the coastline to the abyssal ocean in Figs. 6, 7 and S4. In these profiles, the sediment thickness contribution is shown separately from the ETOPO1 bathymetry. These profiles highlight the fact that the greatest sediment accumulations occur in the shelf-slope-rise regions of the continental margins, whereas open ocean regions accumulate far less. Active margins as in Fig. 6 have thin sediment cover, whereas passive margins as in Figs. 7 and S4 have far thicker sediment cover. On the passive margins, lateral variability in sediment thickness reflects a complex buried topography of the seafloor on which the sediment accumulated. This topography consists of rifted, stretched and sagged lithosphere in km-scale relief, first in-filled by syn-rift sediment and then buried by post-rift sediment (e.g., Watts et al., 2009; Davison and Underhill, 2012). The thickness profiles of the Atlantic margins reflect subsurface graben structures related to the Jurassic-Cretaceous rifting of Pangea (Peron-Pinvidic et al., 2013; Franke, 2013).

The shelf-slope-rise model in Figs. 1 and 8 is based on modern-day bathymetry with three well-defined gradient changes from the coast to the open (deep) ocean. There is no accounting in this model for the complex types of internal architecture in shelf-slope-rise structures just described.

For paleo-ocean reconstructions, extrapolation back through time will produce proportionate narrowing of shelf-slope-rise geometry at passive margins. Highly variable internal structures strongly suggest that simple backward extrapolation may not accurately produce paleo shelf-slope-rise bathymetries, especially for the oldest paleo-oceans. Rifting depends on local lithospheric strength, mantle dynamics, and far field global tectonics, all contributing to the evolution of a passive margin in ways that are not easy to parameterize (Ziegler and Cloetingh, 2003; Corti et al., 2004). Thus, additional

GMDD
8, 3079–3115, 2015

data such as from seismic profiling and ocean margin drill cores must be consulted before applying these types of corrections for deep time reconstructions.

5.2 Residual bathymetry

The Divins sediment thickness (Fig. S2) may be isostatically subtracted from ETOPO1 (Fig. S3) to yield a sediment-stripped bathymetry that should be in isostatic equilibrium with the mantle (Fig. 12a). To detect deviations in this bathymetry from isostatic equilibrium, the OES modeled depth-to-basement (Fig. 4), which is in isostatic equilibrium with the mantle (Eqs. 2 and 3), is subtracted from the sediment-stripped bathymetry. This residual bathymetry (Fig. 12b) is comparable to the residual basement maps of Müller et al. (2008; their Fig. 11), with differences attributable to the isostatic corrections applied to the sediment removal and the predicted crustal (depth-to-basement) models. The unsaturated color range of this map captures many well-known bathymetric anomalies, with the following highlights.

In all oceans, central rift valleys of the mid-ocean ridges have a negative residual bathymetry, not having been modeled by our depth-to-basement procedure. Major transform fault lineaments are negative for the same reason. Otherwise, ridge crests have been successfully removed. Along the central rift valleys there are significant variations, with especially deep values in the southern South Atlantic and Indian Oceans. There is almost no signature of the central rift in the Southern Ocean mid-ocean ridge (between Australia and Antarctica), where sediment cover was underestimated (Divins, 2003).

Most of the eastern Pacific Ocean is close to isostatic equilibrium, but there is broad, low amplitude positive and negative variability throughout the abyssal plains. Elsewhere, hot spots are expressed by long tracks of seamounts, for example the long arcs crossing the southern Pacific Ocean such as the Pukapuka and Louisville seamount chains. The Hawaiian Island chain is surrounded by a pronounced positive swell that is maintained over the entire chain. The western Pacific Ocean has a large

GMDD
8, 3079–3115, 2015

and widespread positive anomaly, some of which is associated with the Ontong-Java Plateau (Taylor, 2012).

Anomalies at ocean margins are evident in the cross-section profiles of Fig. S7, e.g., where ETOPO1 is much shallower (by more than 1.5 km) than OES or EB08. Notable examples are from Newfoundland (Lines 14 and 15) and southeast Africa (Lines 23 and 24), while other examples should not be confused with incompletely modeled delta systems, e.g., the Bay of Bengal (Line 33), or anomalously wide shelves, e.g., the Arctic Ocean margin (Lines 16, 57–59).

Some of the anomalies in the ETOPO1 residual bathymetry may be related to dynamic topography, usually defined as the deviation of surface topography from that expected for the lithosphere in isostatic equilibrium with the underlying mantle (Hager et al., 1985; Braun, 2010; Flament et al., 2013). Dynamic topography is attributed to effects from mass anomalies in the mantle related to mantle convection. Evidence for such mass anomalies comes from the global geoid, which exhibits three large positive anomalies centered on Iceland, the western Pacific Ocean and Southern Ocean near the southern tip of Africa (Cazenave, 1995). Comparison of the residual bathymetry (Fig. 12b) and two slices at +1000 and +2500 m (Fig. S8) identify these three regions as those with the largest positive topographic anomalies worldwide. The northern Atlantic Ocean has the largest positive anomaly, in excess of 2 km, associated with Iceland. Some of this anomaly may be ascribed to the igneous province that comprises Iceland, but the remainder has been explained as dynamic topography resulting from a deep mantle upwelling (Conrad et al., 2004). The western flank of the northern Atlantic Ocean has a large positive anomaly associated with the Bermuda hotspot (Vogt and Jung, 2007). Residual bathymetry also captures part of the African Superswell (Lithgow-Bertelloni and Silver, 1998) around the coast of South Africa and Mozambique, as well as the multiple N–S-trending positive ridges extending offshore from seamounts and hotspot tracks.

The OES bathymetry subjected to the same treatment as ETOPO1 provides a secondary check of our methodology (Fig. 13a). Removing sediments, including their load-

GMDD
8, 3079–3115, 2015

ing, results in a difference map with deeper values than ETOPO1 with the same sediment correction applied (compare Figs. 12a and 13a). This difference also appears in the OES residual bathymetry (Fig. 13b) which shows slightly negative mid-ocean ridges, mostly positive coastlines, and very negative terrigenous sediment fans.

6 Conclusions

The reconstruction method described in this paper was applied to modern data in order to test how well simple parameterizations of the deep and coastal oceans replicate actual modern ocean bathymetry. Our method uses well established components: oceanic crust ages, a cooling plate model, parameterized sediment cover in the open oceans and a parameterized shelf-slope-rise structure based on actual bathymetry from ETOPO1.

Comparison of OES with ETOPO1 bathymetry shows global scale agreement (Fig. 10; Table 3): OES average depth is -3592 ± 1668 m vs. ETOPO1 average depth of -3346 ± 1772 m, a 7.35 % difference; OES median depth is -4321 m vs. ETOPO1 median depth of -3841 m. ETOPO1 is shallower, owing to seamounts and underwater plateaus (LIPs) that are not included in OES bathymetry. OES maximum depth is -6522 m vs. ETOPO1 maximum depth of $-10\,714$ m, reflecting the absence of a full trench model in OES. Significant differences also occur in complex coastal regions north of Siberia, the Falkland Islands, and Indonesia.

OES sediment thickness for the open oceans was parameterized as a multicomponent sediment layer based on a third order polynomial fit between the global ocean sediment thickness data of Divins (2003) and age of the underlying oceanic crust. The OES sediment thickness fits well to Divins sediment thickness in the open oceans, but underestimates Divins sediment thickness at greater ages, especially where terrigenous sediments have accumulated.

The modeled shelf-slope-rise structure for connecting the reconstructed open ocean regions to the continental coastlines was parameterized with respect to adjacent ocean

GMDD
8, 3079–3115, 2015

crustal age and the present-day geometry of the continental shelf-slope-rise. The results show good fits to ETOPO1 for one half of the 64 lines examined from around the world oceans; the other half of the lines examined show moderate to poor fits to ETOPO1.

Residual ocean bathymetry computed from ETOPO1 bathymetry consistently highlights positive anomalies in the North Atlantic Ocean, offshore southeast Africa, and the west Pacific Ocean, where actual bathymetry is elevated more than 1.5 km with respect to that produced by cooling model of the oceanic lithosphere.

It remains unclear whether these differences between true and reconstructed bathymetry produce qualitatively important impacts. One process which for which bathymetry is potentially important is ocean tidal amplitude, which depends sensitively on basin resonances (which in turn depend sensitively on the ocean depth affecting the speed of gravity waves, Arbic et al., 2009). As noted above, both lateral (Krupitsky et al., 1996) and vertical (Sijp and England, 2005) ocean circulation have also been hypothesized be sensitive to the details of bathymetry. Work to evaluate these sensitivities in modern models will be a future focus of research.

The Supplement related to this article is available online at doi:10.5194/gmdd-8-3079-2015-supplement.

Acknowledgements. This work is part of the Open Earth Systems (OES) Project supported by the Frontiers in Earth System Dynamics Program of the US National Science Foundation, Award EAR-1135382. We thank Dietmar Müller (EarthByte) for advice, Christopher R. Scotese (PALEOMAP) for Paleo Atlas data, and Evan Reynolds for technical help throughout the study.

GMDD
8, 3079–3115, 2015

References

Amante, C. and Eakins, B. W.: ETOPO1 1 arc-minute global relief model: procedures, data sources and analysis, US Department of Commerce, NOAA, National Environmental Satellite, Data, and Information Service, NGDC, Marine Geology and Geophysics Division, 2009.

Arbic, B. K., Karsten, R. H., and Garrett, C.: On tidal resonance in the global ocean and the back-effect of coastal tides upon open-ocean tides, Atmos. Ocean, 47, 239–266, doi:10.3137/OC311.2009, 2009.

Braun, J.: The many surface expressions of mantle dynamics, Nat. Geosci., 3, 825–833, 2010.

Cazenave, A.: Geoid, topography and distribution of landforms, Global Earth Physics, 32–39, 1995.

Conrad, C. P., Lithgow-Bertelloni, C., and Louden, K. E.: Iceland, the Farallon slab, and dynamic topography of the North Atlantic, Geology, 32, 177–180, 2004.

Corti, G., Bonini, M., Conticelli, S., Innocenti, F., Manetti, P., and Sokoutis, D.: Analogue modelling of continental extension: a review focused on the relations between the patterns of deformation and the presence of magma, Earth-Sci. Rev., 63, 169–247, 2003.

Crosby, A., McKenzie, D., and Sclater, J.: The relationship between depth, age and gravity in the oceans, Geophys. J. Int., 166, 553–573, 2006.

Crough, S. T.: The correction for sediment loading on the seafloor, J. Geophys. Res.-Sol. Ea., 88, 6449–6454, 1983.

Davison, I. and Underhill, J. R.: Tectonics and Sedimentation in Extensional Rifts, Implications for Petroleum Systems, 2012.

Divins, D.: NGDC total sediment thickness of the world's oceans and marginal seas, NOAA, Boulder, CO, 2008.

Flament, N., Gurnis, M., and Müller, R. D.: A review of observations and models of dynamic topography, Lithosphere, 5, 189–210, 2013.

Franke, D.: Rifting, lithosphere breakup and volcanism: Comparison of magma-poor and volcanic rifted margins, Mar. Petrol. Geol., 43, 63–87, 2013.

Hager, B. H., Clayton, R. W., Richards, M. A., Comer, R. P., and Dziewonski, A. M.: Lower mantle heterogeneity, dynamic topography and the geoid, Nature, 313, 541–545, 1985.

Holbourn, A., Kuhnt, W., and Soeding, E.: Atlantic paleobathymetry, paleoproductivity and paleocirculation in the late Albian: the benthic foraminiferal record, Palaeogeogr. Palaeocl., 170, 171–196, 2001.

GMDD
8, 3079–3115, 2015

Jones, S. M., Lovell, B., and Crosby, A. G.: Comparison of modern and geological observations of dynamic support from mantle convection, J. Geol. Soc. London, 169, 745–758, 2012.
Krupitsky, A., Kamenkovich, V. M., Naik, N., and Cane, M. A.: A linear equivalent barotropic model of the Antarctic circumpolar current with realistic coastlines and bottom topography, J. Phys. Oceanogr., 26, 1803–1824, 1996.
Lithgow-Bertelloni, C. and Silver, P. G.: Dynamic topography, plate driving forces and the African superswell, Nature, 395, 269–272, 1998.
Moucha, R., Forte, A. M., Mitrovica, J. X., Rowley, D. B., Quéré, S., Simmons, N. A., and Grand, S. P.: Dynamic topography and long-term sea-level variations: there is no such thing as a stable continental platform, Earth Planet. Sc. Lett., 271, 101–108, 2008.
Müller, R. D., Sdrolias, M., Gaina, C., and Roest, W. R.: Age, spreading rates, and spreading asymmetry of the world's ocean crust, Geochem. Geophy. Geosy., 9, 1–19, 2008.
Nyblade, A. A. and Robinson, S. W.: The African superswell, Geophys. Res. Lett., 21, 765–768, 1994.
Peron-Pinvidic, G., Manatschal, G., and Osmundsen, P. T.: Structural comparison of archetypal Atlantic rifted margins: a review of observations and concepts, Mar. Petrol. Geol., 43, 21–47, 2013.
Scotese, C. R.: The PALEOMAP Project Paleo Atlas for ArcGIS, Volume 1, Cenozoic Paleogeographic and Plate Tectonic Reconstructions, PALEOMAP Project, Arlington, Texas, 2011.
Shepard, F. P.: Submarine Geology, 3rd edn., Harper and Row, New York, 517 p., 1973.
Sijp, W. and England, M. H.: Role of Drake Passage in controlling the stability of the ocean's thermohaline circulation, J. Climate, 18, 1957–1966, 2005.
Simmons, H. L., Jayne, S. R., St. Laurent, L. C., and Weaver, A. J.: Tidally driven mixing in a numerical model of the ocean general circulation, Ocean Model., 6, 245–263, 2004.
Sykes, T. J.: A correction for sediment load upon the ocean floor: uniform versus varying sediment density estimations – implications for isostatic correction, Mar. Geol., 133, 35–49, 1996.
Taylor, B.: The single largest oceanic plateau: Ontong Java–Manihiki–Hikurangi, Earth Planet. Sc. Lett., 241, 372–380, 2006.
Turcotte, D. L. and Schubert, G. (Eds.): Geodynamics, vol. 1., Cambridge University Press, Cambridge, UK, March 2002, 472 pp., ISBN 0521661862, 2002.
Vogt, P. R. and Jung, W.: Origin of the Bermuda volcanoes and the Bermuda Rise: history, observations, models, and puzzles, Geol. S. Am. S., 430, 553–591, 2007.

GMDD
8, 3079–3115, 2015

Watts, A., Rodger, M., Peirce, C., Greenroyd, C., and Hobbs, R.: Seismic structure, gravity anomalies, and flexure of the Amazon continental margin, NE Brazil, J. Geophys. Res.-Sol. Ea., 114, 1–23, 2009.

Whittaker, J. M., Goncharov, A., Williams, S. E., Müller, R. D., and Leitchenkov, G.: Global sediment thickness data set updated for the Australian-Antarctic Southern Ocean, Geochem. Geophy. Geosy., 14, 3297–3305, 2013.

Winterbourne, J., Crosby, A., and White, N.: Depth, age and dynamic topography of oceanic lithosphere beneath heavily sedimented Atlantic margins, Earth Planet. Sc. Lett., 287, 137–151, 2009.

Wright, J. D. and Miller, K. G.: Control of North Atlantic Deep Water circulation by the Greenland–Scotland Ridge, Paleoceanography, 11, 157–170, 1996.

Ziegler, P. A. and Cloetingh, S.: Dynamic processes controlling evolution of rifted basins, Earth-Sci. Rev., 64, 1–50, 2004.

GMDD

8, 3079–3115, 2015

Table 1. Values for ω_0 and β from Crosby et al. (2006) by ocean basin, and percentage of global ocean areas used to calculate weights for the global averages.

Regions	% of Analyzed Ocean	ω_0 (m)	β ($m s^{-1/2}$)
North Pacific	6.80 %	−2821	−315
Eastern Atlantic	3.38 %	−2527	−336
Southeast Atlantic	4.35 %	−2444	−347
Global Average		−2639.80	−329.50

GMDD
8, 3079–3115, 2015

Table 2. Profile of sediment density vs. depth below sea floor used in our reconstruction. These sediment densities were calculated from a linear extrapolation from the data in Table S1.

Depth (m)	Density of sediment ($kg\,m^{-3}$)
0–100	1670
100–200	1740
200–300	1810
300–400	1880
400–500	1950
500–600	2020
600–700	2090
700–800	2160
800–900	2230
900–1000	2300
1000–1100	2370
1100–1200	2440
1200–1300	2510
1300–1400	2580
1400–1500	2650
> 1500	2720

GMDD
8, 3079–3115, 2015

Table 3. Statistics of three global ocean bathymetries: ETOPO1 is from Amante and Eakins (2009), EB08 is from Müller et al. (2008), and OES model bathymetry is the result of this study. Mean, median, mode, minimum, maximum and SD are in meters; skewness (measure of horizontal symmetry of data distribution) and kurtosis (tall and sharpness of the central peak of data distribution) are dimensionless.

Bathymetry	Max	Min	Average	Median	Mode	SD	Skewness	Kurtosis
OES	−6522.17	204.5	−3591.83	−4321.07	−6.22	1668.52	1.34	3.26
ETOPO1 (ocean only)	−10 714	3933	−3346.41	−3841	−1	1772.25	0.67	2.30
EB08	−5266.97	422.75	−4473.83	−4678.47	−4231.85	785.08	1.81	7.69
ETOPO1 – OES	8812.7	−9231.41	242.53	1.43	5.22	1270.46	0.53	5.71
ETOPO1 – EB08	9129.19	−6349.64	380.93	151.92	108.01	1009.99	1.22	6.40
OES – EB08	5264.95	−4769.50	216.31	169.99	94.59	921.59	1.31	17.12

GMDD
8, 3079–3115, 2015

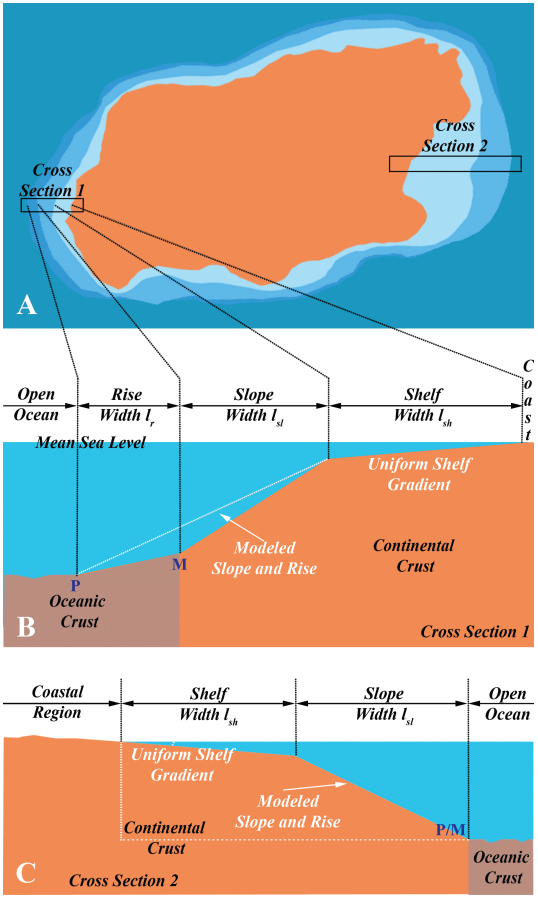

Figure 1. Bathymetric model geometry. **(a)** Map view showing two passive continental margins. Section 1 is a standard passive margin, Sect. 2 is a passive margin with an extended continental shelf. **(b)** Cross section of the standard passive margin with model geometry. **(c)** Cross section of the passive margin with extended continental shelf model geometry.

GMDD
8, 3079–3115, 2015

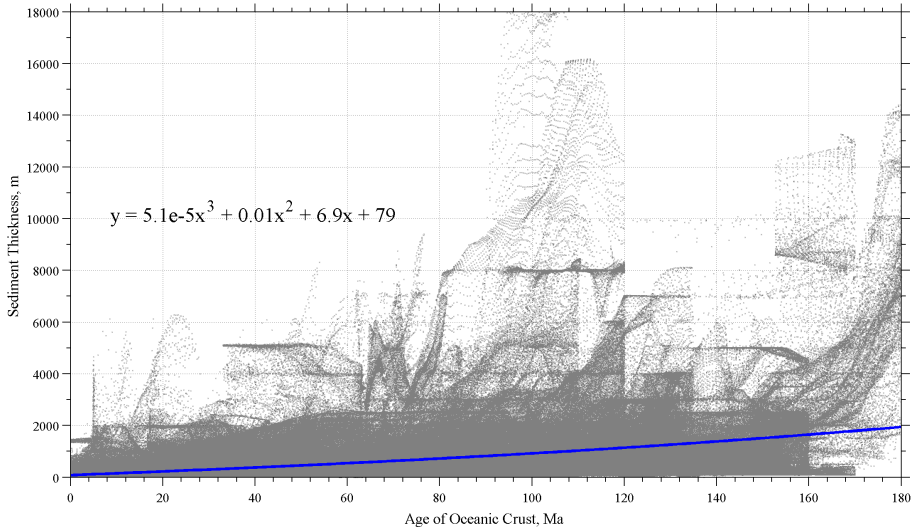

Figure 2. Polynomial fit of sediment thickness as a function of ocean crust age using area corrected global sediment data from Whittaker (2013) and age of the underlying oceanic crust from Müller et al. (2008).

GMDD
8, 3079–3115, 2015

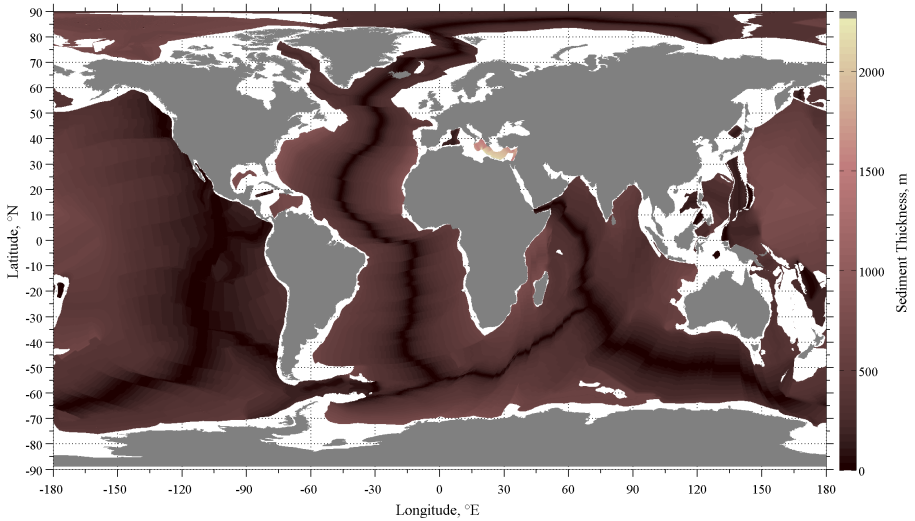

Figure 3. OES model sediment thickness based on the sediment thickness parameterization in Fig. 2.

GMDD
8, 3079–3115, 2015

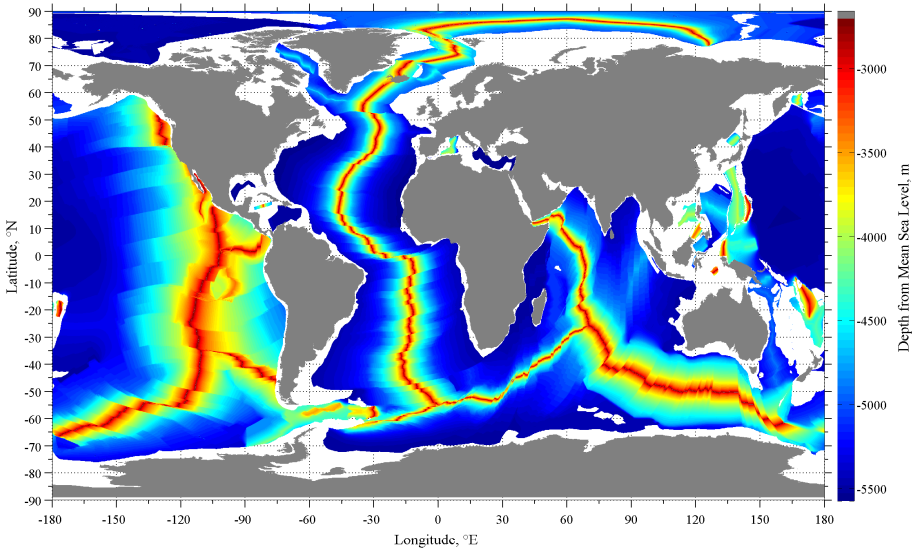

Figure 4. OES model depth-to-basement calculated using Eqs. (1) and (6) and Table 1 in open ocean regions underlain by ocean crust of known age.

GMDD
8, 3079–3115, 2015

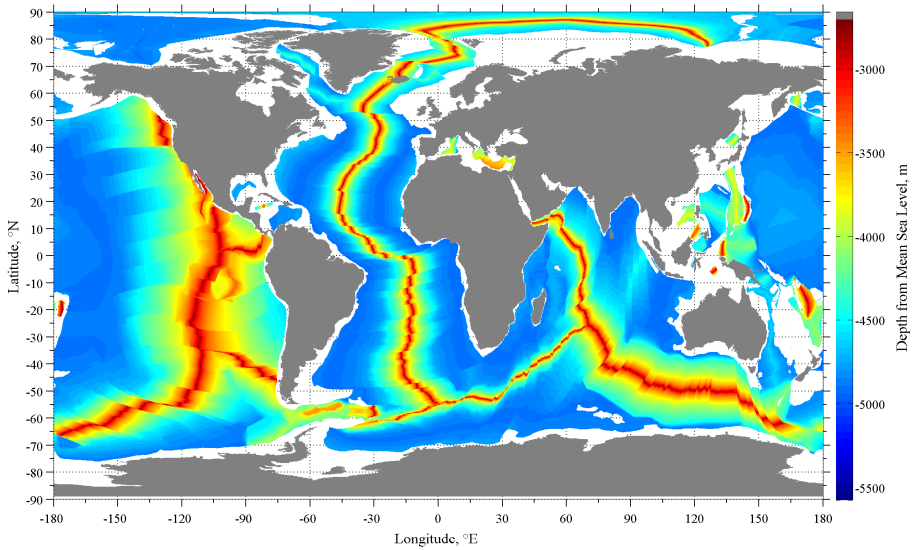

Figure 5. OES model bathymetry for the open ocean regions with isostatically adjusted multicomponent sediment layers of varying densities shown in Table 2. The sediment layer was parameterized as in Fig. 2. The varying sediment densities are from Table 2.

GMDD
8, 3079–3115, 2015

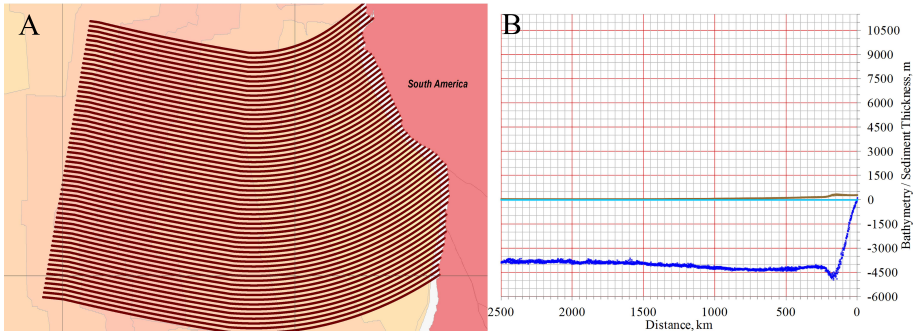

Figure 6. Representative active margin profile off the west coast of South America. **(a)** Transects (brown lines) drawn by smoothly connecting transform fault segments using maps by Scotese (2011). **(b)** Average profile based on all transects in **(a)**. Light blue line represents mean sea level (MSL), brown points represent sediment thickness obtained from Divins (2003) and dark blue points represent bathymetry from ETOPO1.

GMDD
8, 3079–3115, 2015

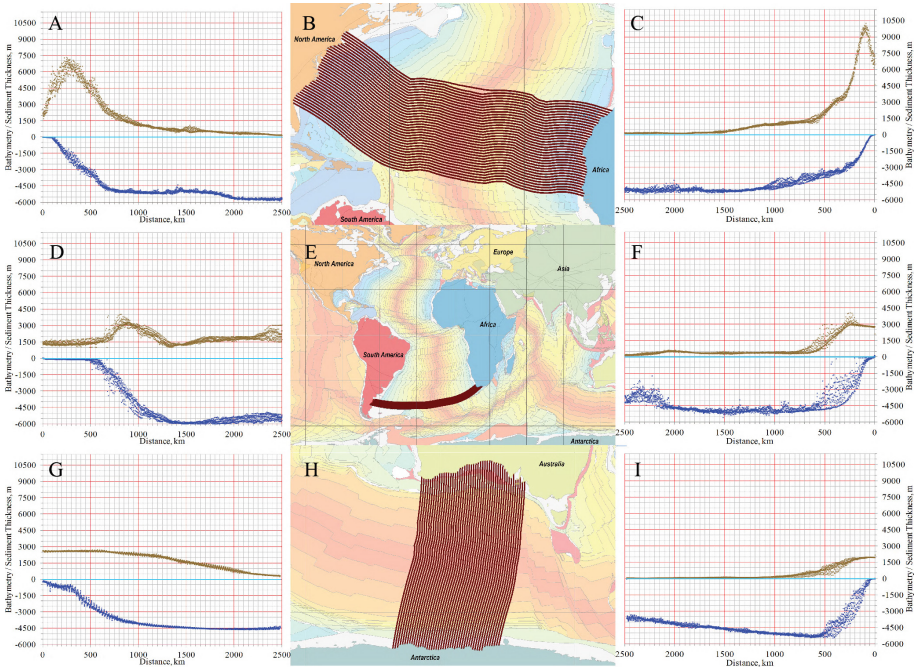

Figure 7. Representative passive margin profiles (shelf-slope-rise structure) from the Atlantic and Southern oceans. (**b, e** and **h**) Transects (brown lines) drawn by smoothly connecting transform fault segments using maps by Scotese (2011). (**a, c, d, f, g** and **i**) Average profiles based on west and east part of all transects in (**b, e** and **h**). Light blue line represents MSL, brown points represent sediment thickness obtained from Divins (2003) and dark blue points represent bathymetry from ETOPO1. Figure S4 displays all 17 transects used.

GMDD
8, 3079–3115, 2015

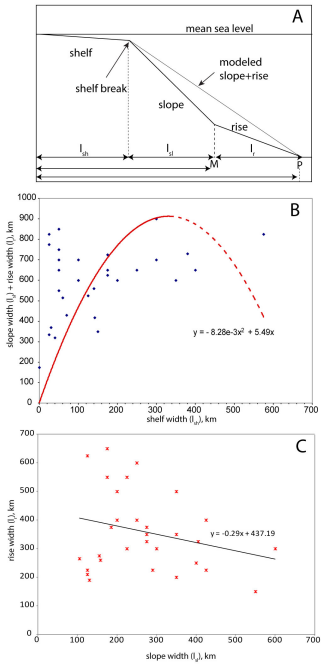

Figure 8. Modeling shelf-slope-rise structure as in Fig. 1. **(a)** The shelf-slope-rise parameterization shown in cross section through a passive continental margin. Parameters are: l_{sh} = continental shelf width; l_{sl} = continental slope width; l_r = rise width; M = maximum extent of oceanic crust (closest to the coastline) from EB08; P = the boundary between the shelf-slope-rise structure and the open ocean. **(b)** Relationship between shelf width (l_{sh}) to slope width + rise width ($l_{sl} + l_r$) in the modern oceans from ETOPO1. Diamonds represent measurements from the east/west coasts of the Atlantic Ocean, and north/south coasts of the Southern Ocean between Australia and Antarctica as shown in Fig. 5. The red line is a parabolic fit; only the solid portion of the fit was used. **(c)** Relationship between slope width (l_{sl}) and rise width (l_r) in the modern oceans from ETOPO1. Red crosses represent measurements at the same locations used in Fig. 8b. The black line is a linear fit.

GMDD
8, 3079–3115, 2015

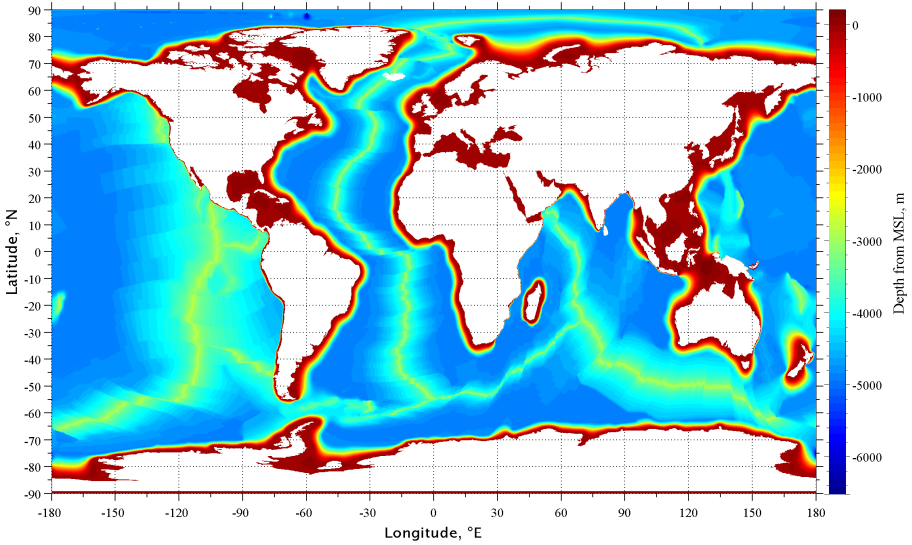

Figure 9. The complete OES model bathymetry including open ocean regions and shelf-slope-rise structures.

GMDD
8, 3079–3115, 2015

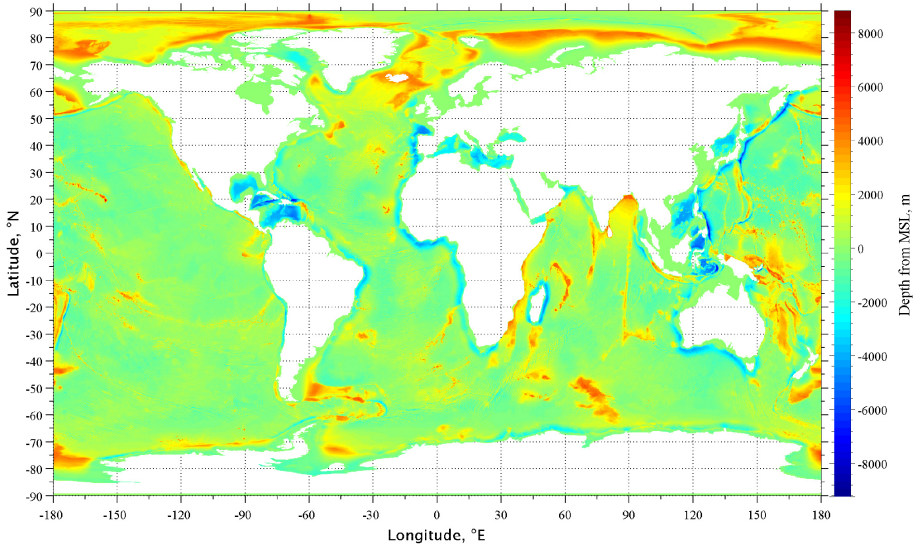

Figure 10. ETOPO1 minus OES model bathymetry. In regions with positive values OES is deeper than ETOPO1, and in regions with negative values OES is shallower than ETOPO1.

GMDD
8, 3079–3115, 2015

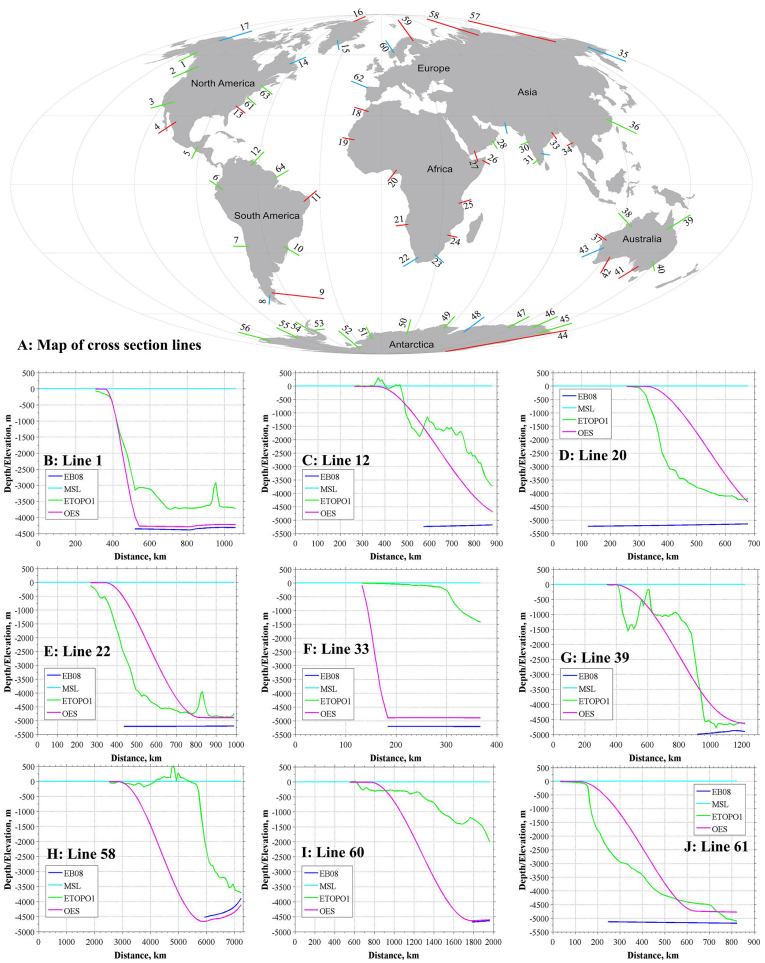

Figure 11. (a) Location of sixty-one profiles comparing OES (Fig. 9) with ETOPO1 and EB08 bathymetries. **(b–j)** Representative profiles at locations shown in Figs. 6 and 7.

GMDD
8, 3079–3115, 2015

OESbathy version 1.0: a method for reconstructing ocean bathymetry

A. Goswami et al.

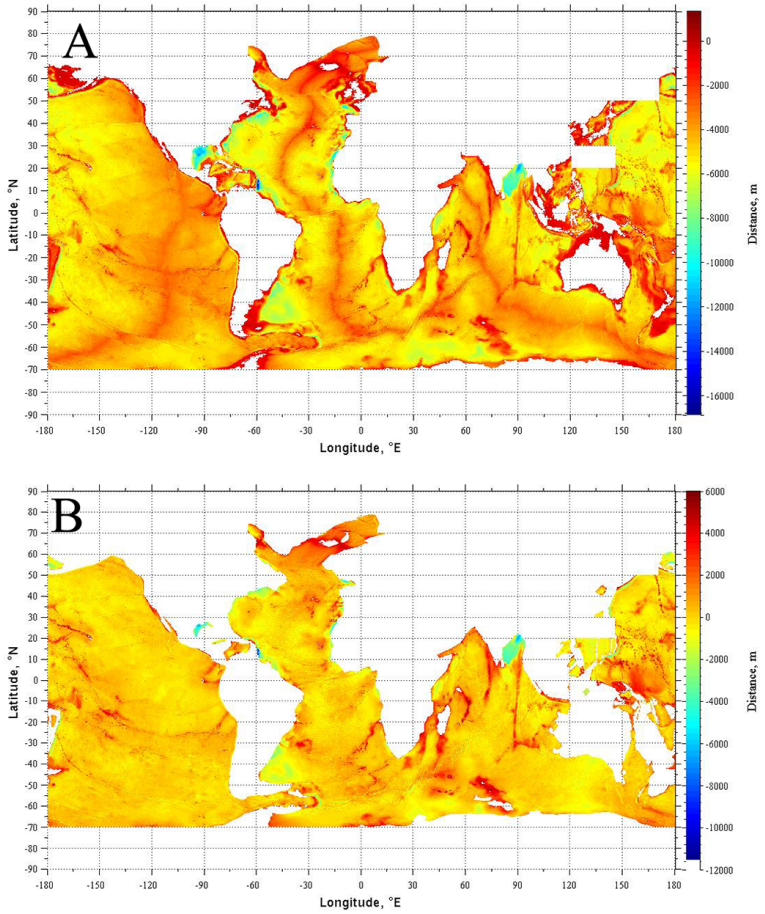

Figure 12. Residual ocean bathymetries: **(a)** ETOPO1 bathymetry minus the global oceanic sediment thickness from Divins (2003) with isostatic re-adjustment applied. **(b)** The bathymetry from **(a)** minus the depth-to-basement bathymetry shown in Fig. 4.

GMDD
8, 3079–3115, 2015

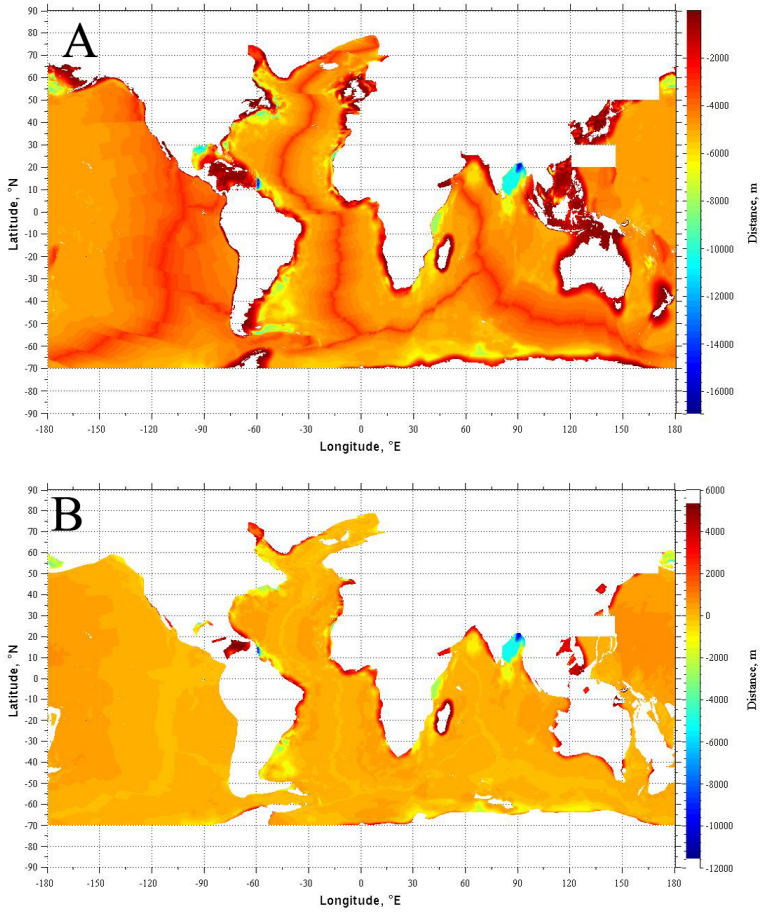

Figure 13. (a) OES model bathymetry minus the global oceanic sediment thickness from Divins (2003) with isostatic correction applied. **(b)** The bathymetry from **(a)** minus the depth-to-basement bathymetry shown in Fig. 4.

GMDD
8, 3079–3115, 2015